Hydrothermally Synthesized Aligned Arrays of Self-Assembled Multiwalled Hydrogen Titanate Nanotubes

ARTICLE *in* CRYSTAL GROWTH & DESIGN · MARCH 2010

Impact Factor: 4.89 · DOI: 10.1021/cg901214a

4 AUTHORS:

Sriparna Chatterjee
Institute of Minerals and Materials Technology
22 PUBLICATIONS **162** CITATIONS
SEE PROFILE

Somnath Bhattacharyya
Indian Institute of Technology Madras
44 PUBLICATIONS **513** CITATIONS
SEE PROFILE

Deepa Khushalani
Tata Institute of Fundamental Research
42 PUBLICATIONS **1,413** CITATIONS
SEE PROFILE

Pushan Ayyub
Tata Institute of Fundamental Research
149 PUBLICATIONS **2,993** CITATIONS
SEE PROFILE

DOI: 10.1021/cg901214a

CRYSTAL GROWTH & DESIGN Article

2010, Vol. 10
1215–1220

Hydrothermally Synthesized Aligned Arrays of Self-Assembled Multiwalled Hydrogen Titanate Nanotubes

Sriparna Chatterjee, Somnath Bhattacharyya, Deepa Khushalani, and Pushan Ayyub*

Tata Institute of Fundamental Research, 1 Homi Bhabha Road, Mumbai 400005, India

Received October 3, 2009; Revised Manuscript Received November 30, 2009

ABSTRACT: We report the hydrothermal synthesis of vertically aligned, multiwalled trititanate ($H_2Ti_3O_7$) nanotube arrays self-assembled on oxidized titanium foils. The growth mechanism is studied in detail using high resolution electron microscopy. We show that a Ti-rich core layer acts as a substrate for the growth of the trititanate nanotube array, whereas the surrounding oxide (rutile) layers serve as the source material. Upon annealing at 500 °C, the 1-D array morphology remains unchanged, but the hollow nanotubes of hydrogen titanate get converted to solid nanorods of TiO_2−B, a low-density titania polymorph. One dimensional arrays of both $H_2Ti_3O_7$ and TiO_2−B are expected to find applications in lithium ion batteries, solar cells, hydrogen sensors, and hydrogen storage and as active catalysts. We provide a straightforward synthesis technique for vertically aligned 1-D arrays of both systems, with excellent adherence to the Ti-rich substrate.

Introduction

One dimensional (1-D) nanostructures—that include quantum wires, nanorods, nanotubes, nanobelts, and nanosprings—are roughly defined as structures whose lateral dimension is limited to about 100 nm. Since the discovery of carbon nanotubes by Iijima in 1991,[1] various 1-D structures continue to attract attention,[2−5] mainly due to their high surface-to-volume ratio, their high aspect ratio, and the unusual nature of electron confinement in them. The synthesis and characterization of several types of oxide nanorods and nanotubes such as TiO_2,[6] ZrO_2,[7] SnO_2,[8] and ZnO[9] have been reported. In particular, the study of arrays of roughly parallel nanorods or nanotubes is of great interest. The properties of a nanorod array (NRA) may differ from those of a single nanorod of the same type in two distinct ways:[10] (a) *additive properties*—an NRA may amplify some advantageous property of a single nanorod and, thus, make it more useful—and (b) *emergent properties*—in certain special cases, an NRA may show distinctly different properties that necessarily involve the presence of the *array*. Additive properties have been utilized while applying ZnO NRAs as UV lasers,[11] photoluminescent sources,[12] photovoltaic cells,[13] field emitters,[14] and gas sensors.[15] Emergent behavior, on the other hand, has been suggested[10] as the reason for metal NRAs exhibiting hydrophobicity[16] and ultralow breakdown voltage in a gas discharge device.[17]

Among various inorganic nanostructures, the TiO_2-based ones have been explored rather extensively because TiO_2 has a high refractive index, an easily tunable wide band gap, very useful catalytic properties, and high thermal and chemical stability. Environmental cleaning using TiO_2 as a photocatalyst is currently an important research area.[18] Clearly, an ordered, vertically oriented TiO_2 nanotube array constitutes an architecture that offers a large internal surface area which dramatically enhances the properties. Thus, a hydrogen sensor based on a 1 μm long titania nanotube array shows an impressive change in the electrical resistivity at room temperature,[19,20] while self-aligned arrays of 45 μm TiO_2 nanorods show a remarkable photoconversion efficiency of 16.25% when used in a photovoltaic device.[21] A TiO_2 based nanotube mesh also shows excellent photovoltaic properties in a dye-sensitized solar cell.[22] In recent years, several authors have discovered a number of promising properties in certain structures related to titania (TiO_2), such as hydrated dititanate ($H_2Ti_2O_5$) and trititanate ($H_2Ti_3O_7$), as well as their Na salts. The most important applications of these *titanate* nanotubes appear to be in sensors,[23] photocatalysts,[24] and electrochromic materials.[25] An aligned array of nanotubes or nanorods (as compared to a nanomesh or a random collection) is particularly useful for applications related to catalysis, gas storage, and gas sensing, because such a geometry provides optimal exposure of the sample surface to the environment. Here, we provide a detailed study of the microstructural evolution of self-aligned, multiwalled, trititanate nanotube arrays during hydrothermal synthesis. On annealing at 500 °C, the $H_2Ti_3O_7$ nanotubes transform to nanorods of TiO_2−B, a low-density titania polymorph with a relatively open structure that allows Li-ion transport and is therefore an attractive candidate for rechargeable Li batteries.[26,27]

The hydrothermal process was used for the synthesis of titania nanotubes in 1999 by Kasuga et al.,[28] while Chen et al.[29] used it to synthesize crystalline trititanate nanotubes and proved that NaOH acts as catalyst as well as reusable source. Later, Armstrong et al. reported the synthesis of TiO_2−B nanowires[30] and nanotubes.[31] The hydrothermal synthesis of titanate nanotubes starting from bulk TiO_2 powder and NaOH was reported in 2006 by Tsai and Teng[32] and Wu et al.,[33] followed the next year by a report on the synthesis and characterization of titanate and titania nanorods.[34] Horvath et al. reported the hydrothermal conversion of titanate nanotubes into nanowires in a revolving autoclave.[35] Guo et al.[36] hydrothermally synthesized titanate nanotube thin films from Ti flakes and NaOH, and they proposed a

*Author to whom correspondence should be addressed. E-mail: Pushan@tifr.res.in.

Published on Web 02/01/2010

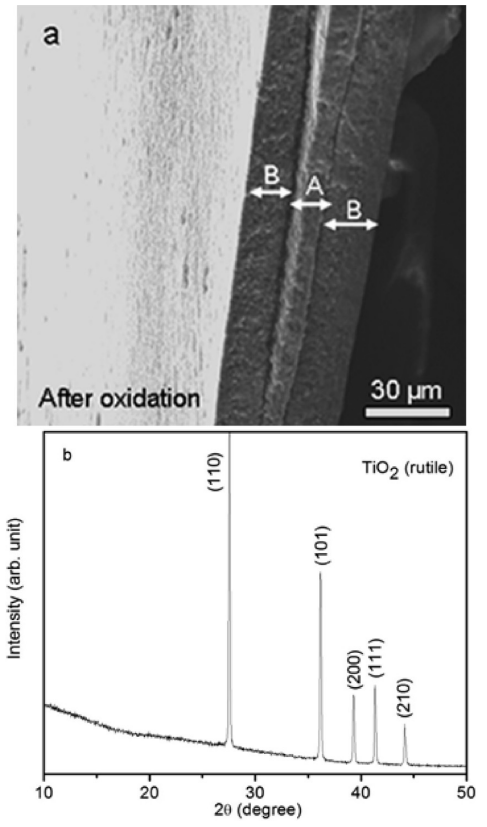

Figure 1. (a) Cross-sectional FE-SEM image of the Ti foil oxidized at 800 °C, where "B" indicates the outer TiO_2 layers, while "A" indicates the Ti rich central layer. (b) XRD pattern of the outer (B) layer showing the pure rutile phase of TiO_2.

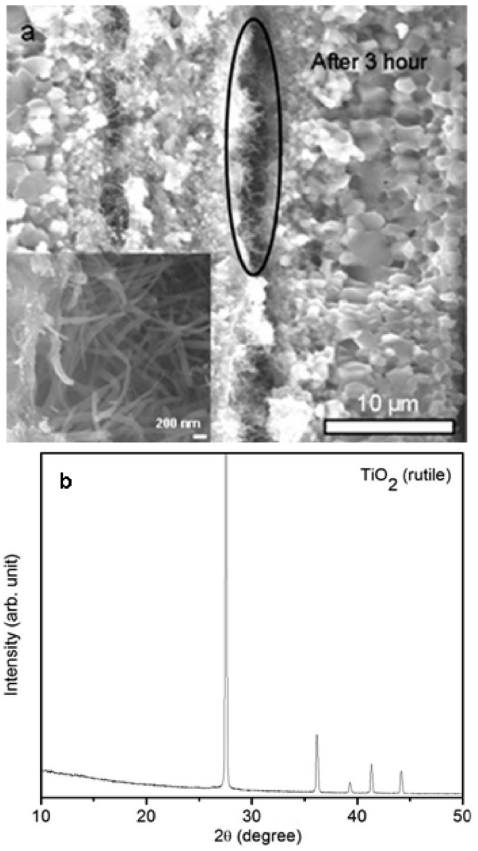

Figure 2. (a) Cross-sectional FE-SEM image of the oxidized Ti foil after hydrothermal treatment for 3 h, showing a similar 3-layer structure as in Figure 1a. The initial stages of the growth of 1-D structures from both surfaces of the central layer can be seen within the outline, and a magnified view is provided in the inset. (b) XRD pattern of the outer layer of this sample, showing the rutile phase.

nanotube growth mechanism. More recently, Shen et al. have shown the hydrothermal splitting of titanate nanowires to a single crystalline titania nanostructure and also measured their photocatalytic activity.[37] In all of the work cited above, the 1-D nanostructures exhibited either imperfect or random alignment. On the other hand, Han et al. synthesized radially aligned TiO_2 based nanorods and investigated their optical properties.[38] Guo et al.[39] have claimed the growth of oriented titante nanotubes on a Ti metal surface, but their cross-sectional scanning electron microscopy (SEM) images do not show a well-defined alignment. Liu et al.[40] synthesized titanate nanorods by high temperature oxidation of Ti chips and proposed a growth mechanism but did not present any cross-sectional SEM images to establish the alignment of the nanorods. Hydrothermal synthesis of well-defined, oriented arrays of titanate nanotubes was reported by Tian et al.,[41] who, however, preseeded their Ti foil with TiO_2 nanoparticles. Therefore, the synthesis of aligned titanate nanotube arrays properly adhering to the substrate (which is important for field emission, photovoltaic, and other applications) is still an unresolved issue.

We report, for the first time, a stepwise study of the hydrothermal synthesis of self-assembled, well-aligned, tri-titanate nanotube arrays from oxidized Ti foils in which *no* preseeding is required. Our study demonstrates that there is a well-defined oxygen gradient along the thickness of the Ti foil, which plays an important role in the growth of the 1-D nanostructure. The Ti-rich central layer acts as a natural substrate for the growth of the nanotube array, while the surrounding TiO_2 layers provide the growth material. Using field emission (FE) SEM as well as high resolution transmission electron microscopy (HR-TEM), we make a detailed study of the growth of the self-assembled $H_2Ti_3O_7$ nanotube array attached to the substrate. In particular, we look at the effect of varying the hydrothermal reaction time and the temperature on the morphology and structure of the nanotubes. The specific advantage of this method is that it can provide self-assembled, well-aligned nanotube arrays of $H_2Ti_3O_7$ as well as nanorod arrays of TiO_2−B, both of which are extremely well anchored to the Ti-rich substrate.

Experimental Methods

The starting material for the synthesis of the aligned titanate nanotube array was a 99.98% pure Ti foil (Sigma-Aldrich, 30 mm × 5 mm × 25 μm), used without further purification. Each foil was oxidized in air in a tube furnace at 800 °C for 5 h, dipped in 35 mL of 10 M NaOH solution in a sealed Teflon reactor, and autoclaved at 200 °C for different durations (1 h, 3 h, 6 h, and 24 h). The samples were washed several times with deionized water and 1:10 HCl successively until the pH of the wash became ≈6.5. The samples were finally washed with hot deionized water to remove any traces of NaCl and then dried at 70 °C. To investigate their thermal stability, the samples were heated briefly to 500 °C at a ramp rate of 5 °C/min.

The crystallographic structure of the product at various stages was investigated using a Panalytical X'pert Pro powder X-ray diffractometer (XRD) with Cu Kα radiation. The elemental

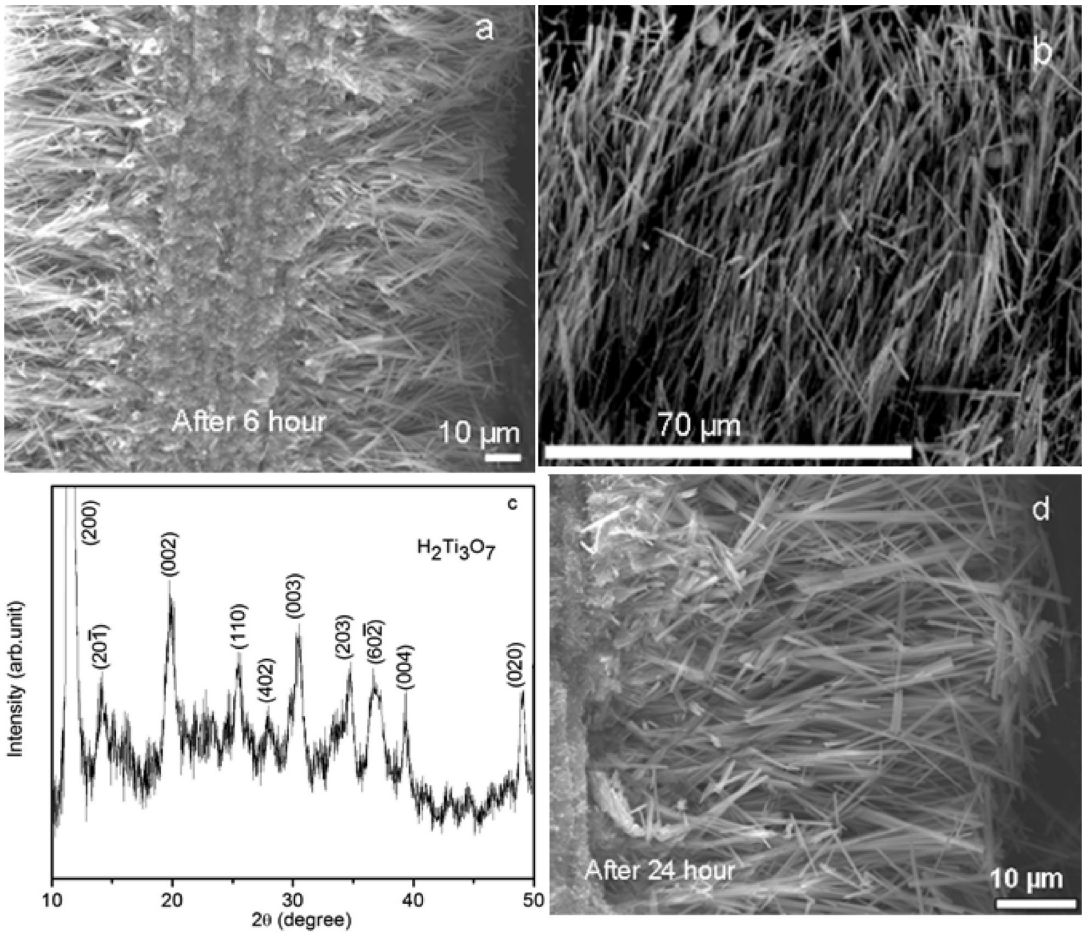

Figure 3. (a) Cross-sectional FE-SEM image of the oxidized Ti foil treated hydrothermally for 6 h, showing fully grown 1-D nanostructured arrays on both sides of the central Ti-rich layer. (b) Plan view of the same sample from one side. (c) XRD pattern of the outer layer of this sample, which can be assigned to the monoclinic trititanate phase. (d) Cross-sectional FE-SEM image of the oxidized Ti foil treated hydrothermally for 24 h (only one side of the central layer is shown at higher magnification).

composition was analyzed by energy dispersive X-ray (EDX) spectroscopy using a Jeol JSM840 SEM. Detailed studies of the microstructure of the samples were performed using an eLiNE FESEM operated at 20 kV. Cross-sectional SEM images were taken at a tilt angle of 89°. The morphology and crystal structure of individual nanotubes and nanorods was studied using a FEI Tecnai-20 transmission electron microscope (TEM) equipped with a LaB_6 filament and operated at 200 kV. Images were recorded on a 1K × 1K slow scan CCD camera and analyzed using the Digital Micrograph software (Gatan Inc., USA). The TEM specimens were prepared by scraping the nanotubes and nanorods off the outer surfaces of the foil, dispersing in ethanol, and placing a drop of the dispersion on a Cu TEM grid covered with a holey carbon film, which was then dried.

Results and Discussions

The cross-sectional SEM image of the oxidized Ti foil (Figure 1a) reveals the presence of three distinct layers, whose compositions were qualitatively analyzed using standardless EDX spectroscopy. The two outer layers of the oxidized foil had almost identical composition with Ti:O ≈ 1:2. However, in the central layer, we observed Ti:O ≈ 7:1. Despite the limitations of this technique, we can conclude that the two outer layers are almost stoichiometric TiO_2, while the central layer is a slightly oxidized metallic Ti phase. Clearly, during the oxidation of the Ti foil, oxygen diffuses in from both the surfaces and creates an oxygen concentration gradient from the outer to the inner parts of the foil, with the inner layer remaining Ti-rich. The steplike variation in the composition across the foil thickness creates a differential thermal expansion in the same direction, since the linear thermal expansion coefficient of TiO_2 is 7.14×10^{-6} K^{-1} while that for pure Ti is 8.6×10^{-6} K^{-1}. During oxidation at 800 °C, the thermal expansion mismatch leads to the generation of extended cracks normal to the cross section of the foil, as seen in Figure 1a. The XRD pattern of both the outer surfaces of the oxidized foil (Figure 1b) completely matches with the tetragonal rutile phase of titania. The X-rays do not penetrate up to the Ti-rich central layer, no evidence of which is therefore seen in the diffraction pattern.

The cross-sectional SEM image of the oxidized Ti foil after 1 h of hydrothermal treatment at 200 °C shows a morphology quite similar to that of the oxidized foil (Figure 1a), while the XRD remains identical to Figure 1b. Hence, there is no appreciable change in morphology and crystal structure of the oxidized foil during the first hour of hydrothermal treatment. The cross-sectional SEM image of a sample that was treated hydrothermally for 3 h is shown in Figure 2a. Here too, one observes the presence of three distinct layers, with the morphology of the outer thick oxide layers remaining unchanged. Interestingly, in this sample one also observes the initial stages of the growth of wirelike structures emanating

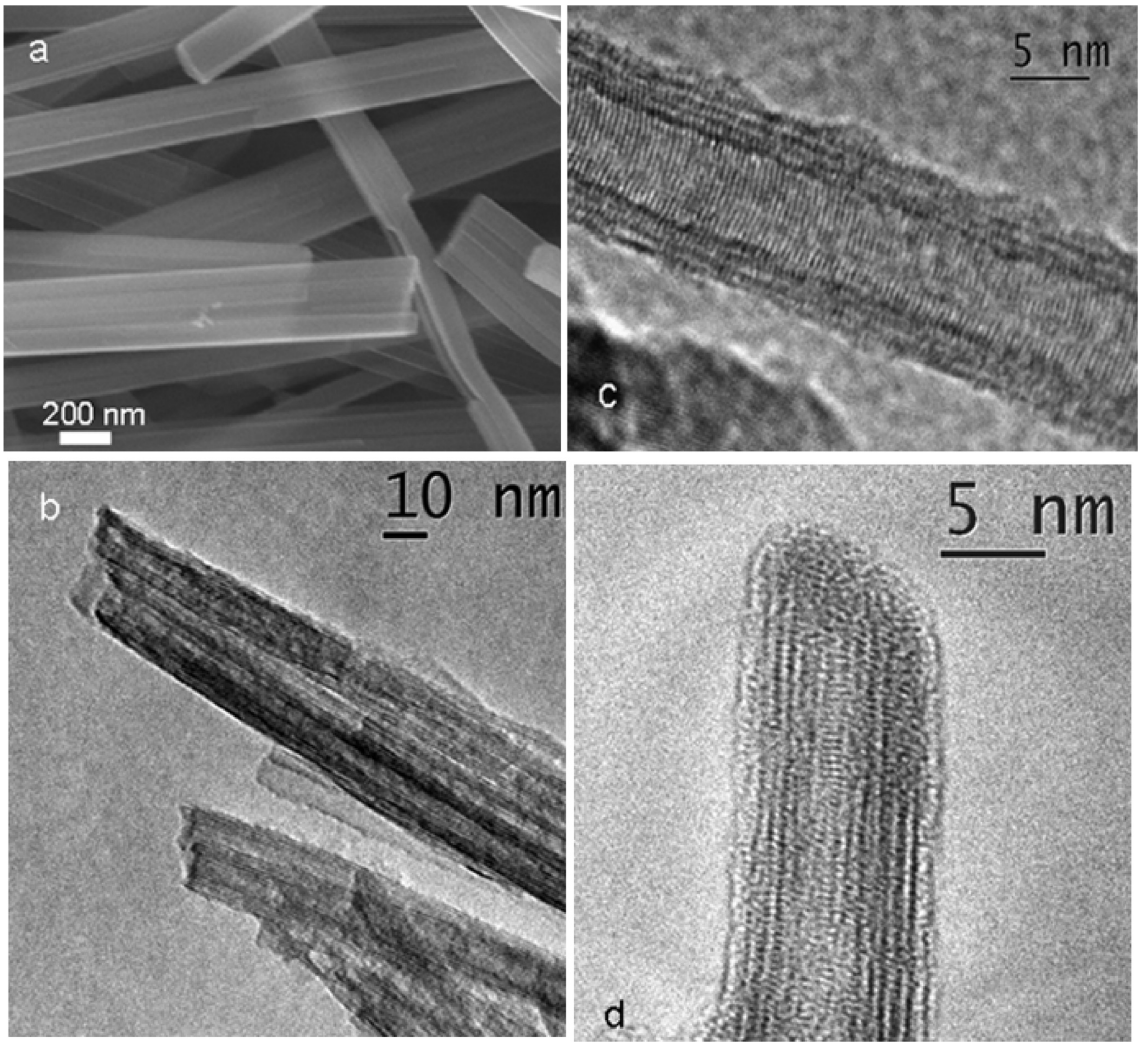

Figure 4. (a) FE-SEM image of the trititanate nanostructures formed on hydrothermal treatment of the oxidized Ti foil for 6 h. (b) TEM image of the bundle-like nanostructures. (c) HR-TEM image showing a single trititanate nanotube that constitutes the bundle. (d) HR-TEM image showing the closed end of such a nanotube.

from both sides of the central layer (see encircled area in Figure 2a). A magnified view of these 1-D structures (inset) shows about 1 μm long wires firmly rooted to the Ti-rich central layer. The XRD spectrum of the outer layers (Figure 2b) again matches with the rutile phase, just as in the as-oxidized foil.

The oxidized foil treated hydrothermally for 6 h exhibits a completely different morphology. The cross-sectional FE-SEM image of this sample (Figure 3a) indicates, first, that the two outer bulk TiO_2 layers are totally absent here. Second, the 1-D nanostructures anchored to the Ti-rich central layer have grown out to a length of about 45 μm on either side, forming large area arrays of roughly parallel 1-D structures, as shown by the plan view SEM in Figure 3b. The XRD spectrum of this sample (Figure 3c) can be satisfactorily assigned to the monoclinic crystal structure of the trititanate ($H_2Ti_3O_7$) phase. The anomalous increase in the (200) reflection indicates a preferential alignment of the nanotubes/nanorods along this direction. There is essentially no further change in the morphology even if the oxidized foil is hydrothermally treated for 24 h, as evidenced by the cross-sectional SEM image of such a sample (Figure 3d). For clarity, only the nanostructure array on one side of the central layer is shown in this high magnification micrograph. The average length of the 1-D structures in this array is still approximately 50 μm. We may therefore conclude that the nanostructure formation starts after about 3 h of hydrothermal processing and almost saturates in about 6 h.

The precise nature of the 1-D structures produced by hydrothermal processing was investigated using high resolution FE-SEM (Figure 4a) and HR-TEM (Figure 4b). Both the SEM and TEM images indicate that each of the 1-D structures is actually a composite of several thinner wirelike units. The HR-TEM image of a single such wirelike unit is most instructive, as it clearly shows that the smallest 1-D units are actually hollow, multiwalled nanotubes. The multiwalled trititanate nanotube shown in Figure 4c has inner and outer diameters of about 5 nm and 10 nm, respectively. This image shows two types of lattices fringes within the nanotube: one along the growth direction, for which the lattice spacing is about 0.8 nm, and another at an angle of about 102°, for which the lattice spacing is about 0.4 nm. These two values correspond closely with the *d*-spacings of the (200) and (003) set of planes in $H_2Ti_3O_7$.[29] The nature of the nanotube walls indicates that the tube formation takes place by a "scrolling" of the multilayer nanosheets, as postulated by previous researchers.[29,36] The

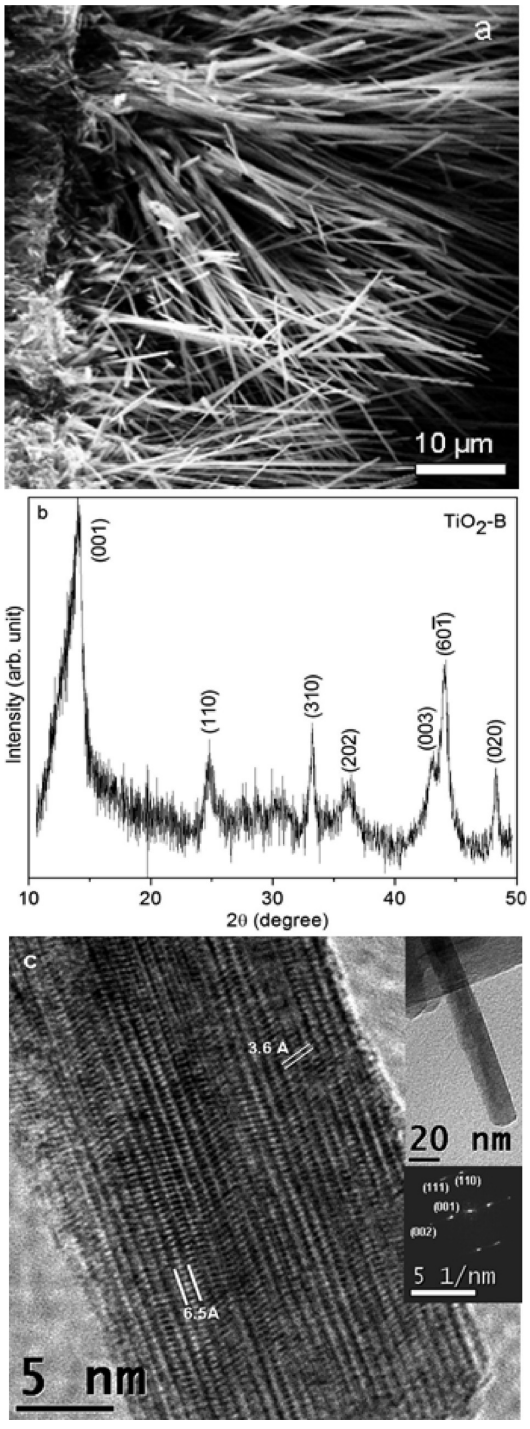

Figure 5. (a) Cross-sectional FE-SEM image of the hydrothermally treated (6 h) sample after annealing at 500 °C, showing the nanorod array on only one side of the central layer. (b) XRD spectrum of the nanorod array, indicating the TiO_2−B phase. (c) High-resolution lattice image of a single TiO_2−B nanorod viewed along the [$\bar{1}$10] direction. The inset (top) shows a low magnification image of the nanorod. The lower inset shows the power spectrum (the square of the magnitude of the complex Fourier transform) of the HRTEM lattice image.

ends of the multiwalled nanotubes observed by us were either broken off or closed. Figure 4d depicts a typical multiwalled nanotube with a closed end.

Our results clearly indicate that the Ti-rich core layer acts as a substrate for the growth of the trititanate nanotube array, whereas the surrounding oxide layers serve as the source material. The hydrothermal synthesis process is performed in a highly alkaline environment, in which TiO_2 can be etched away to form a variety of soluble oxo and hydroxo species, such as $Ti(OH)_2^{2+}$ and $Ti_3O_4^{4+}$. However, these species are expected to be very short-lived and to undergo rapid condensation. Our observations appear to indicate that the Ti-rich inner layer acts a substrate for the preferential nucleation and growth of the $H_2Ti_3O_7$ phase from these soluble precursors. The complete dissolution of the rutile phase takes up to 6 h, and the resulting 1-D trititanate nanostructures grow to a length of about 45−50 μm on either side, even though the initial Ti foil was only 25 μm thick. Since there is no appreciable change when the hydrothermal treatment is carried on beyond 6 h, we may conclude that the outer oxide layers are the main source of the soluble Ti species from which the hydrogen titanate phase is produced and that the almost unoxidized central layer acts as a natural substrate, being itself impervious to base hydrolysis.

To check the robustness of the morphology of the as-prepared trititanate nanotube array, we heated it to 500 °C with a ramp rate of 5 °C min^{-1}, and allowed it to cool immediately. A cross-sectional FE-SEM image of the post-annealed sample (Figure 5a) shows that the basic morphology (aligned 1-D array) is retained. However, the XRD spectrum of the annealed sample (Figure 5b) shows that the $H_2Ti_3O_7$ phase is completely transformed to the TiO_2−B phase. TEM images indicate that the diameters of these structures range from 20 to 100 nm. A high-resolution lattice image of a single 1-D TiO_2−B structure with a diameter of around 20 nm (viewed along the $\bar{1}$10 direction) is shown in Figure 5c, while the upper inset depicts a low magnification image of the entire structure. The lower inset shows the power spectrum of the HRTEM lattice image. Note that the hollow $H_2Ti_3O_7$ nanotubes have been converted to solid TiO_2−B nanorods on instantaneous annealing. Annealing at 500 °C for 12 h produced no substantial change in the structure or composition of the TiO_2−B nanorods, indicating the robustness of the morphology. The thermally induced transformation from $H_2Ti_3O_7$ nanotubes to solid TiO_2−B nanorods is generally due to dehydration followed by local sintering. This phenomenon has been discussed in the literature but does not appear to be completely understood.[42] The complete evolution of the nanostructure with hydrothermal treatment and subsequent annealing is summarized in Table 1.

Existing literature on both nanostructured $H_2Ti_3O_7$ and TiO_2−B suggests that 1-D arrays of these systems can be expected to have a variety of useful applications, particularly in lithium ion batteries, solar cells, hydrogen sensors, and hydrogen storage. In particular, the $H_2Ti_3O_7$ nanotubes are expected to be used as negative electrodes in rechargeable Li-ion batteries, owing to their open, mesoporous structure, efficient Li-ion transport, and good ion-exchange characteristics.[42] Multilayer titania nanotubes are known to accommodate molecular hydrogen over a wide range of temperatures.[43] Titanate nanotubes have a high cation-exchange capacity and may, therefore, be expected to act as active catalysts. Further, nanotube arrays have a very high specific surface area which would facilitate the transport of reagents to the active sites during catalytic reactions.

Table 1. Evolution of the 1-D Nanostructure of the Titania−Trititanate System with Hydrothermal Treatment and Subsequent Annealing

synthesis condition	nature of sample	observed morphology	length of nanotube/rod	diameter of nanotube/rod
oxidation of Ti foil at 800 °C for 5 h	TiO_2 (rutile)	bulk 3-layer structure (TiO_2−Ti−TiO_2)	not present	not present
hydrothermal treatment of oxidized foil in NaOH at 200 °C for 1 h	TiO_2 (rutile)	same as above	not present	not present
hydrothermal treatment of oxidized foil in NaOH at 200 °C for 3 h	TiO_2 (rutile)	initial stages of nanowire formation on the Ti-rich central layer	≈1 μm on both sides of the Ti-rich central layer	∼10 nm
hydrothermal treatment of oxidized foil in NaOH at 200 °C for 6 h	$H_2Ti_3O_7$	nanotube array anchored to the Ti-rich central layer	40−45 μm on both sides of the Ti-rich layer	∼10 nm
hydrothermal treatment of oxidized foil in NaOH at 200 °C for 24 h	$H_2Ti_3O_7$	nanotube array anchored to the Ti-rich central layer	40−50 μm on both sides of the Ti-rich layer	∼10 nm
annealing of 6 h-treated sample at 500 °C	TiO_2−B	nanorod array	40−50 μm	∼20−40 nm

Conclusion

From a detailed study of the hydrothermal growth of TiO_2-based nanostructures from an oxidized Ti foil, we demonstrate that self-assembled, vertically aligned, multiwalled trititanate ($H_2Ti_3O_7$) nanotube arrays grow from a Ti rich substrate layer where the outer oxidized layers act as source material for the growth. The nanotube growth saturates after a threshold reaction time not larger than 6 h. The 1-D array morphology remains unchanged upon annealing at 500 °C, but the crystal structure changes from a monoclinic hydrogen titanate phase to the monoclinic TiO_2−B phase. Because of the simplicity of the synthesis technique, the uniaxial self-alignment and excellent adherence to the substrate, the trititanate nanotube array as well as the TiO_2−B nanorod array may be expected to find a wide range of applications.

Acknowledgment. The authors are grateful to Dr. Mandar Deshmukh for his valuable input and assistance with the FE-SEM experiments. They also thank Mr. Nilesh Kulkarni for his support with XRD experiments.

References

(1) Iijima, S. *Nature* **1991**, *354*, 56.
(2) Hu, J.; Odom, T. W.; Lieber, C. M. *Acc. Chem. Res.* **1999**, *32*, 435.
(3) Xia, Y.; Yang, P.; Sun, Y.; Wu, Y.; Mayers, B.; Gates, B.; Yin, Y.; Kim, Y.; Yan, H. *Adv. Mater.* **2003**, *15*, 353.
(4) Rao, C. N. R.; Deepak, F. L.; Gundiah, G.; Govindaraj, A. *Prog. Solid State Chem.* **2003**, *31*, 5.
(5) Kuchibatla, S. V. N. T.; Karakoti, A. S.; Bera, D.; Seal, S. *Prog. Mater. Sci.* **2007**, *52*, 699.
(6) Guo, Y.-G.; Hu, J.-S.; Liang, H.-P.; Wan, L.-J.; Bai, C.-L. *Adv. Funct. Mater.* **2005**, *15*, 196.
(7) Shin, H.; Jeong, D.-K.; Lee, J.; Sung, M. M.; Kim, J. W. *Adv. Mater.* **2004**, *16*, 1197.
(8) Wang, Y.; Lee, J. Y.; Zeng, H. C. *Chem. Mater.* **2005**, *17*, 3899.
(9) Chatterjee, S.; Gohil, S.; Chalke, B.; Ayyub, P. *J. Nanosci. Nanotechnol.* **2009**, *9*, 4792.
(10) Ayyub, P. *J. Cluster Sci.* **2009**, *20*, 429.
(11) Huang, M. H.; Mao, S.; Feick, H.; Yan, H.; Wu, Y.; Kind, H.; Weber, E.; Russo, R.; Yang, P. *Science* **2001**, *292*, 1897.
(12) Wang, X.; Summers, C. J.; Wang, Z. L. *Nano Lett.* **2004**, *4*, 423.
(13) Law, M.; Greene, L. E.; Johnson, J. C.; Saykally, R.; Yang, P. *Nat. Mater.* **2005**, *4*, 455.
(14) Huang, Y. H.; Zhang, Y.; Liu, L.; Fan, S. S.; Wei, Y.; He, J. *J. Nanosci. Nanotechnol.* **2006**, *6*, 787.
(15) Wang, J. X.; Sun, X. W.; Yang, Y.; Huang, H.; Lee, Y. C.; Tan, O. K.; Vayssieres, L. *Nanotechnology* **2006**, *17*, 4995.
(16) Bhattacharya, P.; Gohil, S.; Mazher, J.; Ghosh, S.; Ayyub, P. *Nanotechnology* **2008**, *19*, 075709.
(17) Carvalho, D.; Ghosh, S.; Banerjee, R.; Ayyub, P. *Nanotechnology* **2008**, *19*, 445713.
(18) Bhattacharya, K.; Varma, S.; Tripathi, A. K.; Bharadwaj, S. R.; Tyagi, A. K. *J. Phys. Chem. C* **2008**, *112*, 19102.
(19) Paulose, M.; Varghese, O. K.; Mor, G. K.; Grimes, C. A.; Ong, K. G. *Nanotechnology* **2006**, *17*, 398.
(20) Mor, G. K.; Varghese, O. K.; Paulose, M.; Grimes, C. A. *Sensor Lett.* **2003**, *1*, 42.
(21) Paulose, M.; Shankar, K.; Yoriya, S.; Prakasam, H. E.; Varghese, O. K.; Mor, G. K.; Latempa, T. A.; Fitzgerald, A.; Grimes, C. A. *J. Phys. Chem. B* **2006**, *110*, 16179.
(22) Flores, I. C.; Freitas, J. N.; Longo, C.; De paoli, M.-A.; Winnischofer, H.; Nogueira, A. F. *J. Photochem. Photobiol. A, Chem* **2007**, *189*, 153.
(23) Liu, A.; Wei, M.; Honma, I.; Zhou, H. *Anal. Chem.* **2005**, *77*, 8068.
(24) Zhang, M.; Jin, Z.; Zhang, J.; Guo, X.; Yang, J.; Li, W.; Wang, X.; Zhang, Z. *J. Mol. Catal. A* **2004**, *217*, 203.
(25) Tokudome, H.; Miyauchi, M. *Angew. Chem., Int. Ed.* **2005**, *44*, 1974.
(26) Armstrong, A. R.; Armstrong, G.; Canales, J.; Garcia, R.; Bruce, P. G. *Adv. Mater.* **2005**, *17*, 862.
(27) Li, Q.; Zhang, J.; Liu, B.; Li, M.; Liu, R.; Li, X.; Ma, H.; Yu, S.; Wang, L.; Zou, Y.; Li, Z.; Zou, B.; Cui, T.; Zou, G. *Inorg. Chem.* **2008**, *47*, 9870.
(28) Kasuga, T.; Hiramatsu, M.; Hoson, A.; Sekino, T.; Niihara, K. *Adv. Mater.* **1999**, *11*, 1307.
(29) Chen, Q.; Zhou, W.; Du, G.; Peng, L.-M. *Adv. Mater.* **2002**, *14*, 1208.
(30) Armstrong, A. R.; Armstrong, G.; Canales, J.; Bruce, P. G. *Angew. Chem., Int. Ed.* **2004**, *43*, 2286.
(31) Armstrong, G.; Armstrong, A. R.; Canales, J.; Bruce, P. G. *Chem. Commun.* **2005**, *19*, 2454.
(32) Tsai, C.-C.; Teng, H. *Chem. Mater.* **2006**, *18*, 367.
(33) Wu, D.; Liu, J.; Zhao, X.; Li, A.; Chen, Y.; Ming, N. *Chem. Mater.* **2006**, *18*, 547.
(34) Kolen'ko, Y. V.; Kovnir, K. A.; Gavrilov, A. I.; Garshev, A. V.; Frantti, J.; Lebedev, O. I.; Churagulov, B. R.; Tendeloo, G. V.; Yoshimura, M. *J. Phys. Chem. B* **2006**, *110*, 4030.
(35) Horváth, E.; Kukovecz, Á.; Kónya, Z.; Kirisci, I. *Chem. Mater.* **2007**, *19*, 927.
(36) Guo, Y.; Lee, N.-H.; Oh, H.-J.; Yoon, C.-R.; Park, K.-S.; Lee, H.-G.; Lee, K.-S.; Kim, S- J. *Nanotechnology* **2007**, *18*, 295608.
(37) Shen, L.; Bao, N.; Zheng, Y.; Gupta, A.; An, T.; Yanagisawa, K. *J. Phys. Chem. C* **2008**, *112*, 8809.
(38) Han, Y.; Li, G.; Zhang, Z. *J. Cryst. Growth* **2006**, *295*, 50.
(39) Guo, Y.; Lee, N.-H.; Oh, H.-J.; Yoon, C.-R.; Park, K.-S.; Jung, S.-C.; Kim, S.-J. *Surf . Coat Technol.* **2008**, *202*, 5431.
(40) Liu, Z.; Yamazaki, T.; Shen, Y.; Meng, D.; Kikuta, T.; Nakatani, N. *J. Phys. Chem. C* **2008**, *112*, 4545.
(41) Tian, Z. R.; Voigt, J. A.; Liu, J.; Mckenzie, B.; Xu, H. *J. Am. Chem. Soc.* **2003**, *125*, 12384.
(42) Bavykin, D. V.; Friedrich, J. M.; Walsh, F. C. *Adv. Mater.* **2006**, *18*, 2807.
(43) Bavykin, D. M.; Lapkin, A. A.; Plucinski, P. K.; Friedrich, J. M.; Walsh, F. C. *J. Phys. Chem. B* **2005**, *109*, 19422.